Néel vector reorientation in ferromagnetic/antiferromagnetic complex oxide nanostructures

A.D. Bang*[1], I. Hallsteinsen[1, 2], F.K. Olsen[1], S.D. Slöetjes[1], S.T. Retterer[3], A. Scholl[2], E. Arenholz[2], E. Folven[1], and J.K. Grepstad[1]

[1] *Department of Electronic Systems, Norwegian University of Science and Technology (NTNU), Trondheim 7491, Norway*
[2]*Advanced Light Source, Lawrence Berkeley National Laboratory, Berkeley, CA 94720, USA*
[3]*Oak Ridge National Laboratory, Oak Ridge, TN 37831, USA*

In this study, we report on a temperature-driven antiferromagnetic (AF) spin reorientation transition in micro- and nanostructures of AF/ferromagnetic (FM) $LaFeO_3/La_{0.7}Sr_{0.3}MnO_3$ thin film bilayers. Using a combination of x-ray photoemission electron microscopy (X-PEEM) and x-ray absorption spectroscopy (XAS), the Néel vector is shown to reorient 90˚ as a result of competition between a shape-imposed anisotropy in the AF layer and interface coupling to the adjacent FM layer. We demonstrate how a temperature dependence of the AF/FM spin configuration in line-shaped nanomagnets can be tuned by variation of their linewidth. This work provides insight into the AF/FM interface exchange coupling in complex oxides heterostructures and the possibilities of spin control by nanostructuring in thin film spintronics.

*ambjorn.bang@ntnu.no

Antiferromagnetic (AF) materials are widely used in advanced magnetic storage and modern sensor devices, primarily serving to pin the magnetization of an adjacent ferromagnet (FM).[1-3] In recent years, the emerging field of AF spintronics promises device applications based solely on antiferromagnets.[4-6] Such AF spintronic devices will rely on accurate control of the AF spin configuration, which is complicated by the absence of net magnetization in these materials.

Recently, current-induced switching of AF spins were demonstrated, relying on spin-orbit torque coupling to the Néel order parameter.[7-9] Another intriguing option to control the Néel vector is introduction of spin reorientation transitions (SRTs) by manipulation of the system anisotropy. In thin film antiferromagnets, the magnetic anisotropy can be engineered through thickness-modulated strain[10-12] or by growth on vicinal substrates.[13,14] In AF/FM bilayer systems with different ordering temperatures of the individual layers, temperature-driven SRTs are possible due to competing anisotropies.[15-18] However, such temperature-driven SRTs have so far been experimentally verified only in the FM layer of an AF/FM bilayer system.[19-21]

Lithographically defined micro- and nanostructures in single-layer films of $LaFeO_3$ (LFO) and in bilayers with $La_{0.7}Sr_{0.3}MnO_3$ (LSMO) have been shown to feature a shape-imposed anisotropy in the AF layer.[22,23] Moreover, this anisotropy is overridden at low temperatures ($T<100$ K) by the interface coupling to the adjacent LSMO layer, reorienting the LFO spins to perpendicular (spin-flop) orientation with respect to the LSMO magnetic moments.[24-27]

In this letter, we present a detailed study of a Néel vector reorientation in LFO/LSMO thin film nanostructures, investigating the effects of temperature, structural dimensions, and applied magnetic fields. Measuring the magnetic linear/circular dichroism (XMLD/XMCD) in the x-ray absorption using both x-ray photoemission electron microscopy (X-PEEM) and x-ray absorption spectroscopy (XAS), the AF/FM spin configuration were examined for a wide range of sample temperatures (50 – 300 K). We find an in-plane AF SRT within a narrow temperature range, which is shifted by varying the lateral dimensions of these thin film nanostructures.

*ambjorn.bang@ntnu.no

The LFO/LSMO bilayer films were grown epitaxially on (001)-oriented, Nb-doped (0.05 wt %) $SrTiO_3$ substrates, using growth parameters reported elsewhere.[23,28] The individual layers were 90 unit cells (u.c.) thick (1 u.c. ≈ 0.4 nm) for the FM (LSMO) layer and 10 u.c. thick for the AF (LFO) layer. Nano- and microstructures were created in these thin films by first defining a protective mask of either resist (CSAR62) or metal (Cr) using electron beam lithography. Subsequent exposure to Ar^+ ion bombardment serves to disrupt the magnetic order in unmasked regions, and following removal of the mask leaves nano- and micromagnets embedded in a paramagnetic matrix.[22,29] Two different types of line patterns were examined in this work. For the X-PEEM measurements, we defined "square wave" line structures of different linewidths. For the XAS measurements, we prepared extended arrays of straight lines covering an area of 1 x 2 mm^2, so as to accommodate the full spot of the incident x-ray beam. The line patterns were oriented along the magnetocrystalline easy axes of LSMO, i.e. the in-plane (pseudocubic) <110> directions.[30,31] Magnetometry measurements (not shown) after the patterning process showed no appreciable reduction of the Curie temperature, measured at T_C = 360 K for blanket films. For the LFO layer, we assume a Néel temperature well above room temperature, estimated at $T_N \approx 640$ K for blanket films.[32,33]

The measurements were carried out at the Advanced Light Source (ALS) using the PEEM3 end station (beamline 11.0.1) for X-PEEM and the Magnetic Spectroscopy and Scattering beamline 4.0.2 for XAS. The ultra-thin (10 u.c.) thickness of the AF top layer ensures photoemission sensitivity to Mn $L_{2,3}$ absorption in the underlying FM layer, and thus permits selective probing of the magnetic order in the two layers. In X-PEEM, FM domain contrast was obtained from magnetic circular dichroism at the Mn L_3 absorption edge, and AF domain contrast was obtained from magnetic linear dichroism in the absorption of s-polarized x-rays tuned to the two maxima of the Fe L_2 multiplet. In the XAS measurements on beamline 4.0.2, XMLD and XMCD spectra were obtained from the x-ray absorption spectra measured (via total electron yield) across the Fe $L_{2,3}$ edge and the Mn $L_{2,3}$ edge, respectively. The vector magnet on the 4.0.2. end station allows for XAS measurements to be carried out in an applied magnetic field.

*ambjorn.bang@ntnu.no

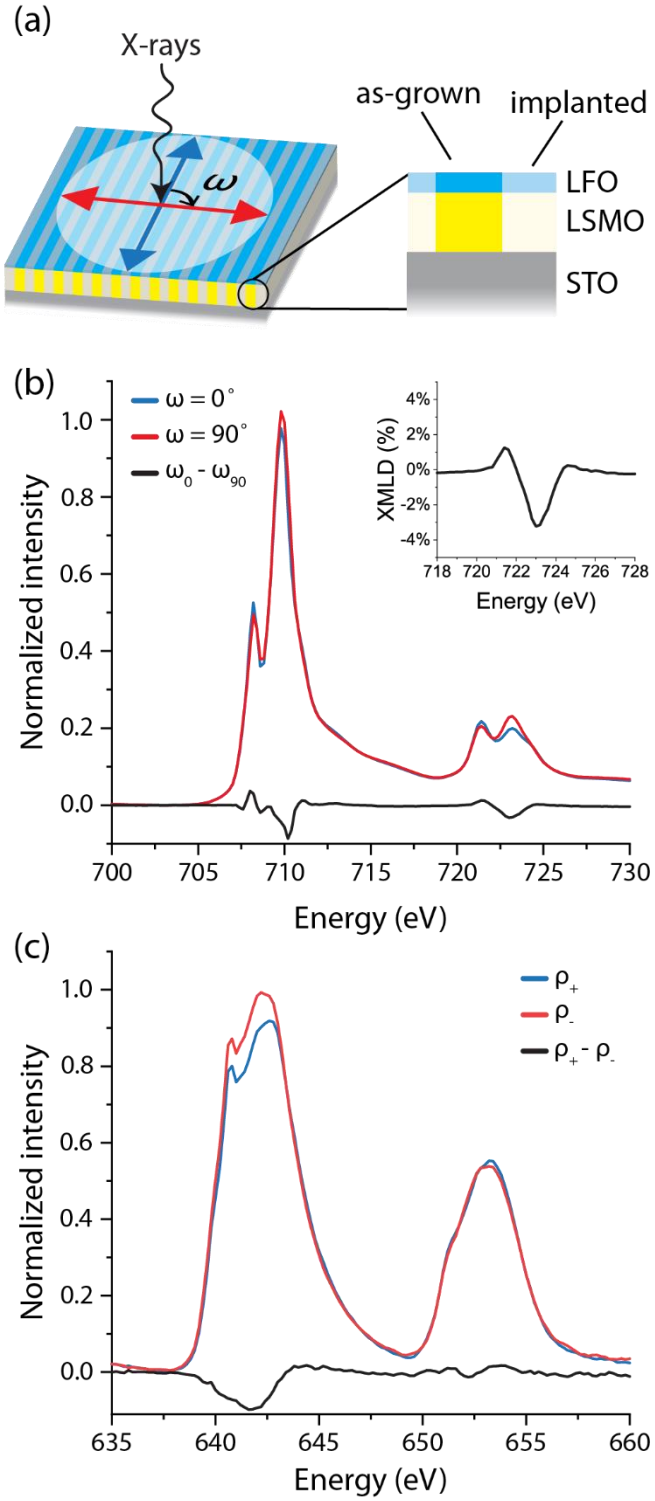

Figure 1: XAS spectra recorded for an extended 450 nm linewidth line pattern at 50 K. (a) schematic depicting the experimental set-up used for the XAS XMLD measurements. The blue (red) arrow designates the polarization plane for ω = 0° (ω = 90°). (b) Fe $L_{2,3}$ x-ray absorption and XMLD spectra measured in normal incidence. The inset shows the XMLD signature of the Fe L_2 peak. (c) Mn $L_{2,3}$ x-ray absorption and XMCD spectra measured at 30° (grazing) incidence parallel to the patterned lines. ρ_+ and ρ_- refer to right- and left-handed circularly polarized x-rays, respectively.

*ambjorn.bang@ntnu.no

Figure 1a depicts the experimental geometry for the XMLD XAS measurements. The incident x-ray spot (~100×100 μm^2) was focused fully within the line pattern arrays to ensure that the data originates solely from the structured region of the sample. The spectra were recorded in normal incidence with the E-vector parallel ($\omega = 0^\circ$) and perpendicular ($\omega = 90^\circ$) to the line pattern, respectively. It should be noted that the absorption spectrum for these extended line arrays is a superposition of spectra from as-grown thin film and implanted material.

Figure 1b shows the x-ray absorption spectra for $\omega = 0^\circ$ and $\omega = 90^\circ$, and the resulting XMLD (difference) spectrum recorded at 50 K for a linewidth of 450 nm. A distinct linear dichroism is observed in the XMLD spectrum, suggesting AF order with a predominant Néel vector orientation. Absorption spectra recorded for both an all-implanted film region and an unpatterned (blanket film) region showed no dichroism (see Supplementary information), confirming that the measured dichroism derives from the line pattern. XMLD at the Fe $L_{2,3}$ edge has been found to depend on the crystalline environment of the $Fe^{2+/3+}$ ions, and the XMLD signature was shown to change sign dependent on the in-plane orientation of the AF spin axis with respect to the crystal axes.[34-36] With both the E-vector of the incident x-rays and the patterned lines oriented along in-plane <110> directions, the XMLD spectrum shown in the inset of figure 1b implies that the Néel vector is predominantly oriented perpendicular to the lines.

Figure 1c shows x-ray absorption spectra obtained for right- and left-handed circularly polarized x-rays (ρ_+ and ρ_-) incident at 30° with the sample surface and the plane of incidence parallel to the line structures. Also shown is the corresponding XMCD (difference) spectrum, which by comparison with in-field measurements on single-layer LSMO blanket films (see Supplementary information) indicates magnetization parallel to the lines, as expected from shape anisotropy. The AF/FM spin alignment is thus perpendicular (spin-flop), in keeping with previous reports for this thin film bilayer system at comparable temperatures.[24,25] We note that the LSMO absorption spectrum includes an unconventional feature at ~ 640 eV, which derives from the implanted matrix. Ion implantation of LSMO films has been shown to shift the valency of Mn from primarily Mn^{3+}/Mn^{4+} to also include a significant fraction of Mn^{2+}.[37] The observed absorption spectrum fits a superposition of the XAS spectra recorded for implanted and blanket films, respectively (see Supplementary information).

*ambjorn.bang@ntnu.no

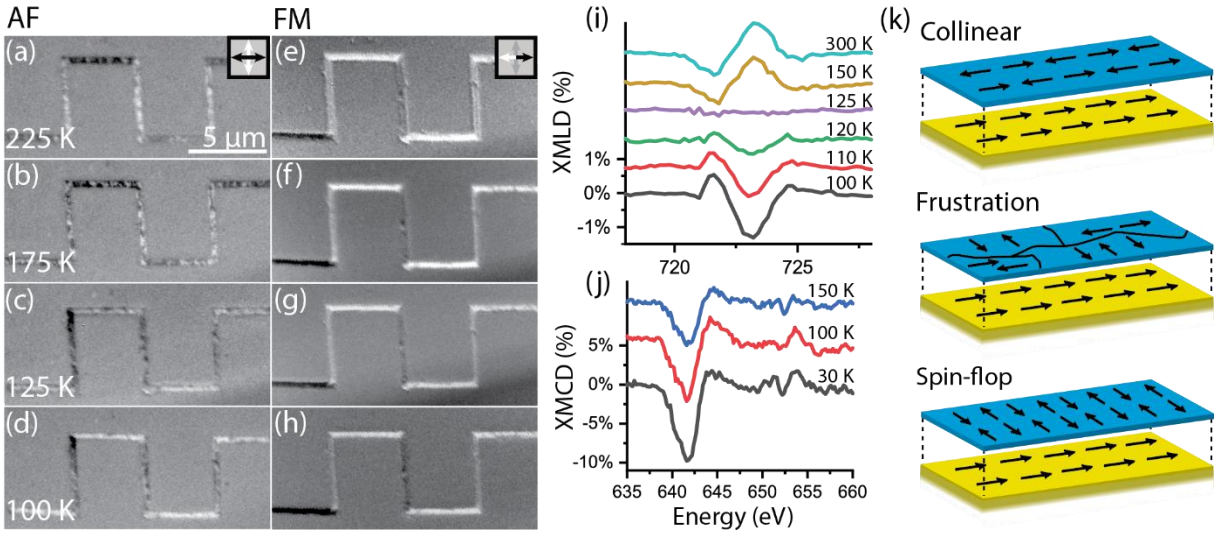

Figure 2: X-PEEM images and XAS XMLD/XMCD spectra recorded at different temperatures, showing the AF/FM spin alignment through the SRT. (a-h) AF and FM domain patterns of 500 nm wide «square wave» line structures. Legends indicating the correspondence between X-PEEM domain contrast and direction of magnetization apply to all four images in each column; (i) XMLD spectra of the Fe L_2 edge and (j) XMCD spectra of the Mn $L_{2,3}$ edge, recorded at different temperatures above and below the SRT temperature; (k) schematic of the different AF/FM spin configurations of this SRT

The X-PEEM and XAS data in figure 2(a-j) display a distinct temperature dependence of the AF/FM spin configuration, shifting from collinear to spin-flop alignment of the Néel vector and the FM moments within the temperature range 100 – 200 K. Figure 2(a-d) shows AF domain patterns for a 500 nm wide ”square wave” line structure oriented along in-plane <110> directions. For temperatures above 225 K, the predominant orientation of the AF spin axis is parallel to the lines, in keeping with earlier observations of shape-imposed AF domain formation for similar structures.[23,24] At T = 175 K (figure 2b), while maintaining a predominance of parallel-oriented AF domains, formation of new domains with their spin axis oriented perpendicular to the “square wave” line is observed. When lowering the temperature to T = 125 K (figure 2c), a substantial fraction of the AF spins is oriented perpendicular to the FM moments, which invariably align parallel to the lines due to shape anisotropy, cf. figure 2(e-h). With reduction of the sample temperature to T = 100 K, the recorded AF domain pattern (figure 2d) shows a distinct spin-flop configuration of the FM moments and the AF spin axis. No further changes to the XMLD-PEEM images were observed upon lowering the temperature to T = 30 K.

*ambjorn.bang@ntnu.no

The recorded temperature dependence of the AF/FM spin axis alignment is corroborated by XMLD/XMCD spectra recorded for the extended line arrays of 450 nm linewidth (figure 2i-j). In figure 2i, the XMLD spectrum of the Fe L_2 peak is shown for temperatures from 100 – 300 K. At T = 300 K, the XMLD signature is consistent with an AF spin axis oriented parallel to the lines. At T = 125 K, the XMLD signal completely disappears, which indicates a frustrated domain state with a 50/50 distribution of AF domains with the Néel vector oriented respectively perpendicular and parallel to the lines. Finally, at T = 100 K, we record the XMLD signature of a fully perpendicular (spin-flop) alignment. The XMCD spectra recorded at the Mn L_3 edge confirm magnetization parallel to the lines throughout the entire temperature range (cf. figure 2j). The AF/FM spin alignment thus changes from collinear via frustrated to perpendicular orientation with decreasing temperature, as depicted in the schematic of figure 2k.

In the AF layer, we identify three factors contributing to the AF spin alignment; the intrinsic magnetocrystalline anisotropy, the shape-imposed anisotropy associated with extended domains forming along the micro-/nanostructure edges,[22-24] and the interface exchange coupling to the adjacent FM LSMO layer.[24,25] Grown epitaxially on LSMO/STO(001), the AF domain pattern of ultrathin (10 u.c.) blanket LFO films were found to exhibit magnetic domains with the AF spin axis oriented along both <100> and <110> (pseudocubic) in-plane crystalline directions,[23,38] suggesting magnetocrystalline easy axes along these four directions. In patterned lines oriented along in-plane <110> crystalline directions, parallel and perpendicular orientation of the LFO Néel vector with respect to the line edges are thus equally preferred by the magnetocrystalline anisotropy. In contrast, the anisotropy imposed by the nanostructure edges favors parallel alignment of the Néel vector in these lines, in competition with the interface exchange coupling, which favors perpendicular (spin-flop) alignment of the Néel vector and the FM moments in the LSMO layer. The latter are strongly confined by shape anisotropy to be oriented parallel with the lines. The results shown in figure 2 indicate that the shape-imposed (edge) anisotropy predominates at elevated temperatures ($T \geq 225$ K) with collinear alignment of the FM moments and the AF spin axis. However, below some critical temperature, the interface exchange coupling overcomes this shape-effect, rotating the AF spin axis 90° to perpendicular (spin-flop) orientation with the FM moments.

*ambjorn.bang@ntnu.no

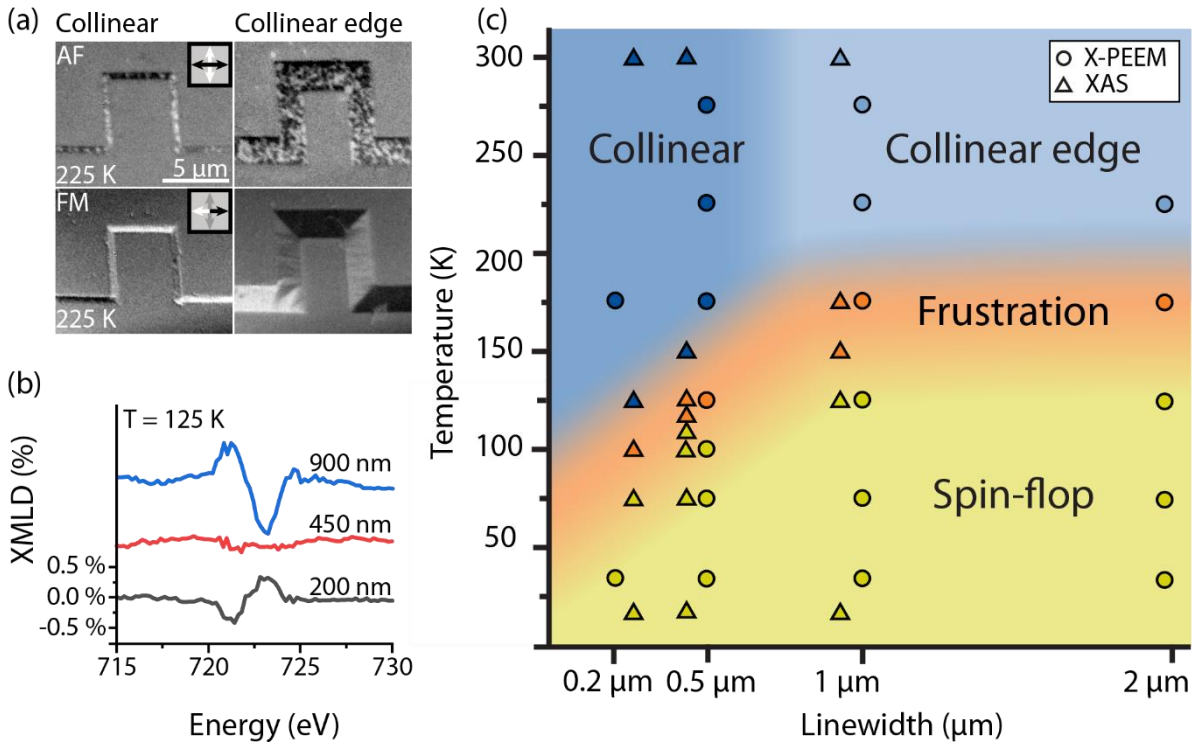

Figure 3: Linewidth and temperature dependence of the AF/FM spin alignment. (a) X-PEEM images of the AF and FM domain patterns, demonstrating the difference between the characteristic AF domain patterns of a comparatively wide (2 µm) and a narrow (500 nm) line at elevated temperature (225 K, above the SRT). Legends in the two leftmost images indicate the correspondence between X-PEEM domain contrast and direction of magnetization and apply to all four images. (b) XMLD spectra of the Fe L_2 edge for three different linewidths at 125 K. (c) Compilation of data from the recorded X-PEEM images and XMLD spectra in a linewidth–temperature phase diagram for the AF/FM spin alignment.

Figure 3 shows the impact of the linewidth for the AF/FM spin configuration in these LFO/LSMO bilayer line patterns. We note from the XMLD-PEEM image of the 2 µm wide line in figure 3a, that the AF edge domains, with their spins aligned collinearly with the FM moments, extend no more than ~300 nm into the line. Beyond this limit, the domain pattern changes to that characteristic of an LFO blanket film.[32,39] In line structures with a width ≤ 500 nm, the AF edge domains extend throughout the full width of the lines, effectively dominating the AF domain pattern. We thus distinguish between two characteristic AF domain patterns above the SRT temperature, i.e., "collinear edge" alignment for linewidths ≥ 1 µm, and "collinear" alignment for linewidths ≤ 500 nm.

The linewidth is observed to have a profound impact on the spin reorientation temperature. At T = 125 K, the XMLD spectra in figure 3b are characteristic of spin-flop, frustration, and collinear alignment of the AF/FM spin configuration for line structures of linewidths 900, 450, and 200 nm, respectively. We can thus observe the three stages of the SRT for one and

*ambjorn.bang@ntnu.no

the same temperature, by variation of the linewidth. Combining data from X-PEEM and XAS measurements, the AF/FM spin configuration for different linewidths is assessed for a wide range of sample temperatures and classified according to the categories ‘collinear’, ‘frustrated’, and ‘spin-flop’ alignment. A compilation of this data is presented in the linewidth–temperature phase diagram in figure 3c. (The X-PEEM images and XMLD-PEEM spectra used to compile this phase diagram are provided in Supplementary information.)

The phase diagram in figure 3c distinguishes between two distinct regimes of the AF domain pattern above the SRT temperature. In line structures where the AF domain pattern is characterized by collinear AF/FM spin alignment along the edges only, the SRT temperature appears to be independent of the linewidth. When collinear AF/FM spin alignment extends throughout the full width of the lines, this configuration is preserved to a lower temperature. The SRT temperature is dependent on the linewidth, with the Néel vector in 200 nm wide lines switching to spin-flop configuration at lower temperature than in the 500 nm wide lines. Gomonay et al.[33] have proposed a model taking surface magnetic anisotropy and long-range magnetoelastic forces into account, predicting a shape-dependent magnetic anisotropy in AF nanoparticles. We note that this model predicts a stronger shape-imposed anisotropy for thinner lines, consistent with our findings.

As the interface exchange coupling forcing the transition to spin-flop alignment of the AF spin axis and FM moments apparently grows stronger with decreasing temperature, we investigated whether this coupling could be related to the LSMO volume magnetization. Figure 4 shows the impact of a 0.3 T magnetic field applied parallel to the 450 nm wide lines for sample temperatures below, near, and above the SRT. This external field was oriented at an angle of 20˚ with the sample surface to avoid trapping of emitted low-energy electrons, so as to maximize the electron yield. A magnetic field of this magnitude is presumed to have negligible effect on the AF layer, as spin reorientation in antiferromagnets typically requires magnetic fields in excess of several Tesla.[40,41] Magnetometry data (not shown) for these patterned samples show that the difference in LSMO volume magnetization between measurements in remanence and at an applied field of 0.3 T exceeds the increase in volume magnetization when reducing the sample temperature from 150 K to below 50 K. The XMLD spectra in figure 4 are virtually identical to those measured in zero field, and demonstrates that a 0.3 T applied field has no observable impact on the AF/FM spin alignment in this

*ambjorn.bang@ntnu.no

system. Thus, this SRT does not seem to depend on the magnitude of the LSMO volume magnetization.

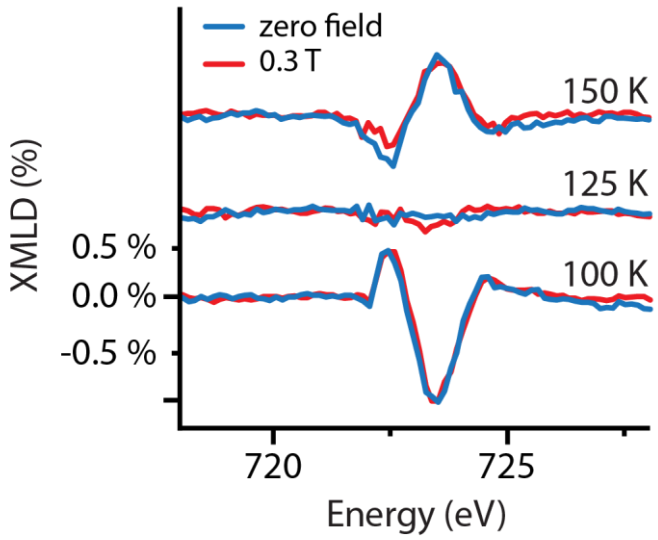

Figure 4: Comparison of XMLD spectra recorded at the Fe L_2 edge, with and without an external applied field.

In summary, we have investigated a temperature-driven Néel vector reorientation in patterned line structure arrays defined in LFO/LSMO bilayer films. This SRT is shown to originate from a competition between a shape-imposed anisotropy in the AF layer and the interface exchange coupling between the two layers. The FM moments remain fixed by shape anisotropy, causing the AF/FM alignment to change gradually from collinear to perpendicular (spin-flop) dependent on the sample temperature. The transition temperature was found to decrease with the linewidth in lines thinner than ~500 nm. Measurements carried out in an applied magnetic field show no impact on this SRT. The present findings shed light on the nature of SRTs in patterned AF/FM complex oxide heterostructures and demonstrate the possibilities offered by nanostructuring to control the magnetic spin configuration in such bilayer systems.

Supplementary Material

See supplementary material for XAS spectra obtained from LFO and LSMO reference thin films and the additional X-PEEM and XAS data used to compile the phase diagram in figure 3.

*ambjorn.bang@ntnu.no

Acknowledgments

This research was undertaken with financial support from the Research Council of Norway, under grant no. 231290. Partial funding was also obtained from the Norwegian PhD Network on Nanotechnology for Microsystems (A.D.B.), which is sponsored by the Research Council of Norway, Division for Science, under contract no. 221860/F60. The Advanced Light Source is supported by the Director, Office of Science, Office of Basic Energy Sciences, and the U.S. Department of Energy under contract DE-AC02-05CH11231. Nanoscale patterning was carried out in part at the Center for Nanophase Materials Sciences, which is a U.S. DOE Office of Science User Facility, and at NTNU NanoLab, NorFab. The Research Council of Norway is acknowledged for the support to the Norwegian Micro- and Nanofabrication Facility, NorFab, project number 245963/F50

[1] J. Nogués and I. K. Schuller, Journal of Magnetism and Magnetic Materials **192** (2), 203 (1999).

[2] M. Kiwi, Journal of Magnetism and Magnetic Materials **234** (3), 584 (2001).

[3] W. Zhang and K. M. Krishnan, Materials Science and Engineering: R: Reports **105**, 1 (2016).

[4] T. Jungwirth, X. Marti, P. Wadley, and J. Wunderlich, Nature Nanotechnology **11** (3), 231 (2016).

[5] T. Jungwirth, J. Sinova, A. Manchon, X. Marti, J. Wunderlich, and C. Felser, Nature Physics **14** (3), 200 (2018).

[6] E. V. Gomonay and V. M. Loktev, Low Temperature Physics **40** (1), 17 (2014).

[7] S. Yu Bodnar, L. Šmejkal, I. Turek, T. Jungwirth, O. Gomonay, J. Sinova, A. A. Sapozhnik, H. J. Elmers, M. Kläui, and M. Jourdan, Nature Communications **9** (1), 348 (2018).

[8] P. Wadley, B. Howells, J. Železný, C. Andrews, V. Hills, R. P. Campion, V. Novák, K. Olejník, F. Maccherozzi, S. S. Dhesi, S. Y. Martin, T. Wagner, J. Wunderlich, F. Freimuth, Y. Mokrousov, J.

*ambjorn.bang@ntnu.no

Kuneš, J. S. Chauhan, M. J. Grzybowski, A. W. Rushforth, K. W. Edmonds, B. L. Gallagher, and T. Jungwirth, Science **351** (6273), 587 (2016).

[9] M. J. Grzybowski, P. Wadley, K. W. Edmonds, R. Beardsley, V. Hills, R. P. Campion, B. L. Gallagher, J. S. Chauhan, V. Novak, T. Jungwirth, F. Maccherozzi, and S. S. Dhesi, Physical Review Letters **118** (5), 057701 (2017).

[10] J. Zhu, Q. Li, J. X. Li, Z. Ding, C. Y. Hua, M. J. Huang, H. J. Lin, Z. Hu, C. Won, and Y. Z. Wu, Journal of Applied Physics **115** (19), 193903 (2014).

[11] J. Li, E. Arenholz, Y. Meng, A. Tan, J. Park, E. Jin, H. Son, J. Wu, C. A. Jenkins, A. Scholl, H. W. Zhao, C. Hwang, and Z. Q. Qiu, Physical Review B **84** (1), 012406 (2011).

[12] W. Kim, E. Jin, J. Wu, J. Park, E. Arenholz, A. Scholl, C. Hwang, and Z. Q. Qiu, Physical Review B **81** (17), 174416 (2010).

[13] Y. Z. Wu, Z. Q. Qiu, Y. Zhao, A. T. Young, E. Arenholz, and B. Sinkovic, Physical Review B **74** (21), 212402 (2006).

[14] Q. Li, T. Gu, J. Zhu, Z. Ding, J. X. Li, J. H. Liang, Y. M. Luo, Z. Hu, C. Y. Hua, H. J. Lin, T. W. Pi, C. Won, and Y. Z. Wu, Physical Review B **91** (10), 104424 (2015).

[15] P. J. Jensen and H. Dreyssé, Physical Review B **66** (22), 220407 (2002).

[16] P. J. Jensen, H. Dreyssé, and M. Kiwi, The European Physical Journal B - Condensed Matter and Complex Systems **46** (4), 541 (2005).

[17] F. I. F. Nascimento, Ana L. Dantas, L. L. Oliveira, V. D. Mello, R. E. Camley, and A. S. Carriço, Physical Review B **80** (14), 144407 (2009).

[18] J. H. Seok, H. Y. Kwon, S. S. Hong, Y. Z. Wu, Z. Q. Qiu, and C. Won, Physical Review B **80** (17), 174407 (2009).

[19] W. Zhang and K. M. Krishnan, Physical Review B **88** (2), 024428 (2013).

[20] J. Li, M. Przybylski, F. Yildiz, X. L. Fu, and Y. Z. Wu, Physical Review B **83** (9), 094436 (2011).

[21] Q. Zhan and K. M. Krishnan, Applied Physics Letters **96** (11), 112506 (2010).

*ambjorn.bang@ntnu.no

[22] E. Folven, T. Tybell, A. Scholl, A. Young, S. T. Retterer, Y. Takamura, and J. K. Grepstad, Nano Letters **10** (11), 4578 (2010).

[23] E. Folven, A. Scholl, A. Young, S. T. Retterer, J. E. Boschker, T. Tybell, Y. Takamura, and J. K. Grepstad, Physical Review B **84** (22), 220410 (2011).

[24] E. Folven, A. Scholl, A. Young, S. T. Retterer, J. E. Boschker, T. Tybell, Y. Takamura, and J. K. Grepstad, Nano Letters **12** (5), 2386 (2012).

[25] Y. Takamura, E. Folven, J. B. R. Shu, K. R. Lukes, B. Li, A. Scholl, A. T. Young, S. T. Retterer, T. Tybell, and J. K. Grepstad, Physical Review Letters **111** (10) (2013).

[26] M. S. Lee, T. A. Wynn, E. Folven, R. V. Chopdekar, A. Scholl, S. T. Retterer, J. K. Grepstad, and Y. Takamura, Physical Review Materials **1** (1), 014402 (2017).

[27] A. D. Bang, F. K. Olsen, S. D. Slöetjes, A. Scholl, S. T. Retterer, C. A. F. Vaz, T. Tybell, E. Folven, and J. K. Grepstad, Applied Physics Letters **113** (13), 132402 (2018).

[28] J. E. Boschker, E. Folven, Å. F. Monsen, E. Wahlström, J. K. Grepstad, and T. Tybell, Crystal Growth & Design **12** (2), 562 (2012).

[29] Y. Takamura, R. V. Chopdekar, A. Scholl, A. Doran, J. A. Liddle, B. Harteneck, and Y. Suzuki, Nano Letters **6** (6), 1287 (2006).

[30] P. Lecoeur, P. L. Trouilloud, Gang Xiao, A. Gupta, G. Q. Gong, and X. W. Li, Journal of Applied Physics **82** (8), 3934 (1997).

[31] M. Mathews, F. M. Postma, J. C. Lodder, R. Jansen, G. Rijnders, and D. H. A. Blank, Applied Physics Letters **87** (24), 242507 (2005).

[32] A. Scholl, J. Stöhr, J. Lüning, J. W. Seo, J. Fompeyrine, H. Siegwart, J.-P. Locquet, F. Nolting, S. Anders, E. E. Fullerton, M. R. Scheinfein, and H. A. Padmore, Science **287** (5455), 1014 (2000).

[33] J. K. Grepstad, Y. Takamura, A. Scholl, I. Hole, Y. Suzuki, and T. Tybell, Thin Solid Films **486** (1), 108 (2005).

*ambjorn.bang@ntnu.no

[34] S. Czekaj, F. Nolting, L. J. Heyderman, P. R. Willmott, and G. van der Laan, Physical Review B **73** (2), 020401 (2006).

[35] E. Arenholz, G. van der Laan, R. V. Chopdekar, and Y. Suzuki, Physical Review B **74** (9), 094407 (2006).

[36] E. Arenholz, G. van der Laan, F. Yang, N. Kemik, M. D. Biegalski, H. M. Christen, and Y. Takamura, Applied Physics Letters **94** (7), 072503 (2009).

[37] M. S. Lee, Doctoral thesis, University of California, Davis (2018).

[38] E. Folven, Y. Takamura, and J. K. Grepstad, Journal of Electron Spectroscopy and Related Phenomena **185** (10), 381 (2012).

[39] S. Czekaj, F. Nolting, L. J. Heyderman, K. Kunze, and M. Krüger, Journal of Physics: Condensed Matter **19** (38), 386214 (2007).

[40] G. R. Hoogeboom, A. Aqeel, T. Kuschel, T. T. M. Palstra, and B. J. van Wees, Applied Physics Letters **111** (5), 052409 (2017).

[41] A. A. Sapozhnik, R. Abrudan, Y. Skourski, M. Jourdan, H. Zabel, M. Kläui, and H. J. Elmers, physica status solidi (RRL) – Rapid Research Letters **11** (4), 1600438 (2017).

*ambjorn.bang@ntnu.no

Supplementary Information for:

Néel vector reorientation in ferromagnetic/ anti-ferromagnetic complex oxide nanostructures

A.D. Bang*[1], I. Hallsteinsen[1, 2], F.K. Olsen[1], S.D. Slöetjes[1], S.T. Retterer[3], A. Scholl[2], E. Arenholz[2], E. Folven[1], and J.K. Grepstad[1]

[1] *Department of Electronic Systems, Norwegian University of Science and Technology (NTNU), Trondheim 7491, Norway*
[2]*Advanced Light Source, Lawrence Berkeley National Laboratory, Berkeley, CA 94720, USA*
[3]*Oak Ridge National Laboratory, Oak Ridge, TN 37831, USA*

*ambjorn.bang@ntnu.no

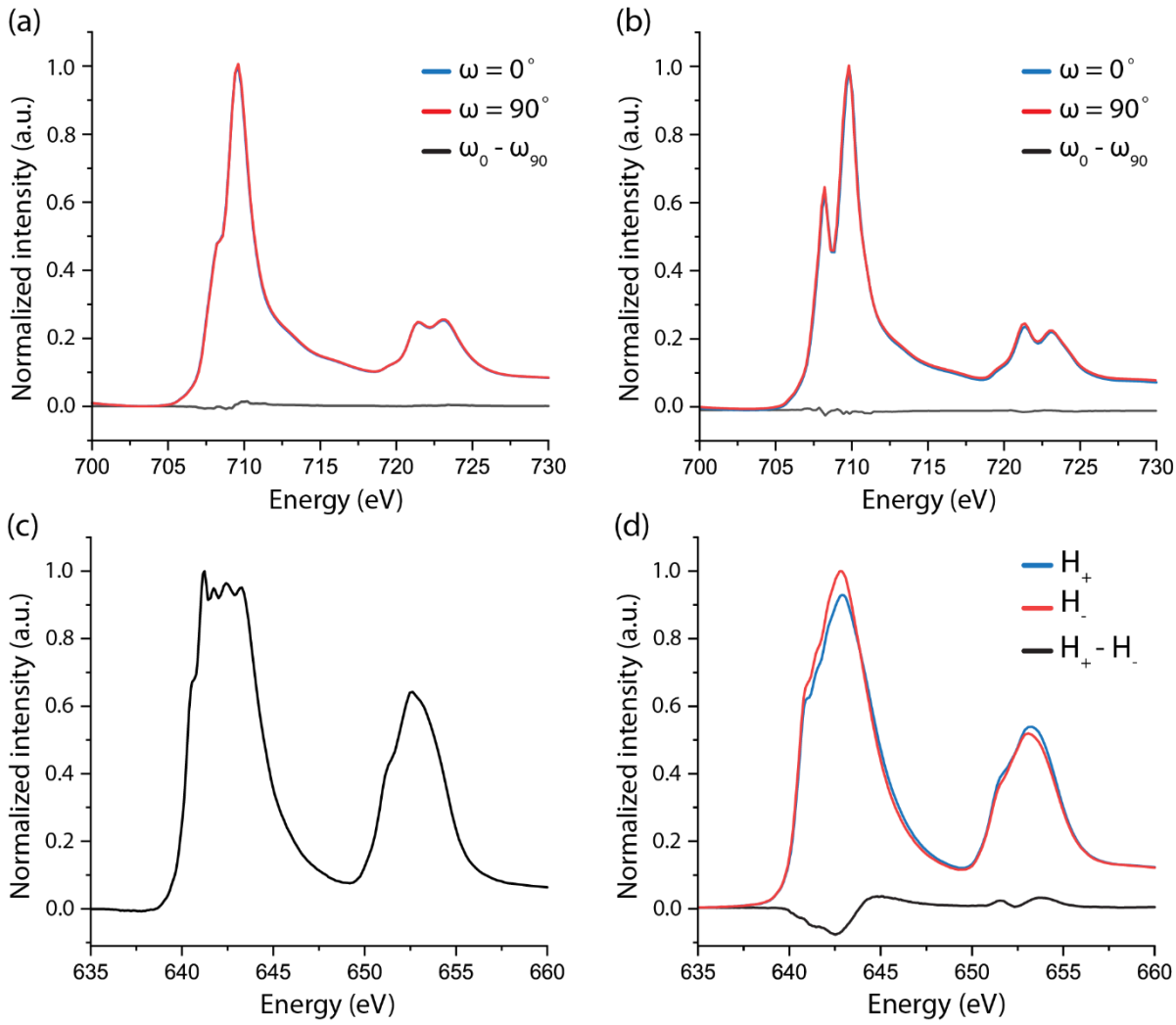

Figure S1: XAS spectra recorded for thin film reference samples of (a) all-implanted 10 u.c. LFO, with corresponding XMLD spectrum, (b) unpatterned 10 u.c. LFO, with corresponding XMLD spectrum, (c) all-implanted 90 u.c. LSMO, and (d) unpatterned 90 u.c. LSMO, with corresponding XMCD spectrum. H_+ and H_- in (d) refer to a positive and a negative orientation of the magnetic holding field, where the positive direction is defined as parallel to the incident x-rays.

In order to better understand the characteristics of the x-ray absorption spectra obtained from patterned regions of the LFO/LSMO bilayer samples (roughly 50/50 implanted/as-grown material), we measured the Fe $L_{2,3}$ and Mn $L_{2,3}$ spectra from two reference samples of LFO and LSMO, respectively, cf. figure S1. Figure S1a-b show XAS spectra from a 10 u.c. single-layer of LFO, obtained for an Ar^+-ion implanted and an unpatterned (blanket) film region, respectively. A negligible dichroism signature is observed for the unpatterned LFO layer measured in normal incidence of the x-ray beam. Deposited on STO(001), ultrathin (10 u.c.) layers of LFO feature a pattern of sub-μm AF domains with their spin axis oriented along the in-plane (pseudocubic) <110> and <100> crystalline directions in equal shares.[1] Due to the

*ambjorn.bang@ntnu.no

comparatively large probing area of the incident x-ray beam (~100×100 μm^2), the XMLD signal is thus expected to average zero for a blanket film at normal incidence.

Figure S1c-d show XAS spectra obtained for an Ar^+ ion implanted and an unpatterned film region of a 90 u.c. single-layer film of LSMO. In order to obtain a measureable XMCD signature from an unpatterned LSMO region, a magnetic holding field of 0.3 T was used. The XMCD signal is found by subtraction of two absorption spectra recorded with right-handed circularly polarized x-rays, where the holding field was applied parallel and antiparallel to the incident x-rays. The XAS spectrum from the implanted region (figure S1c) shows a pronounced peak broadening of the Mn L_3 peak. This signature is attributed to an increased fraction of Mn^{2+} in the implanted material.[2]

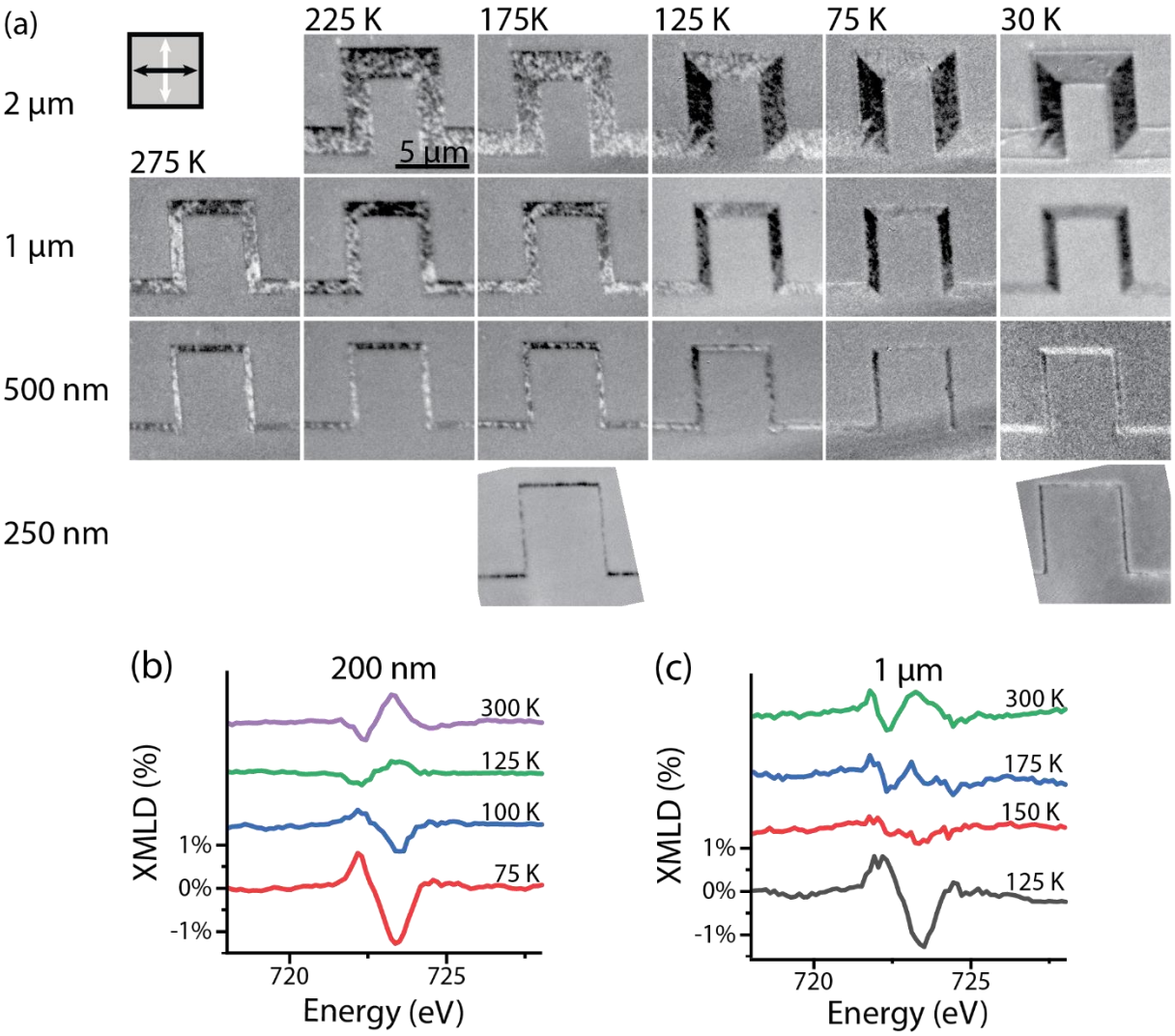

Figure S2: XMLD-PEEM images and XMLD spectra showing the AF spin orientation for different linewidths. (a) XMLD-PEEM images showing the AF domain pattern at different temperatures for «square wave» line structures of different linewidths. (b) and (c) show the XMLD spectra recorded at different temperatures for extended line arrays with linewidth of 200 nm and 1 μm, respectively.

*ambjorn.bang@ntnu.no

Figure S2 summarizes the data used to compile the phase diagram (figure 3) in the main paper. Only XMLD-PEEM data from the AF layer is shown here (figure S2a), as the XMCD-PEEM data shows the FM moments to always be aligned parallel to the lines for all linewidths and temperatures.

[1] E. Folven, A. Scholl, A. Young, S. T. Retterer, J. E. Boschker, T. Tybell, Y. Takamura, and J. K. Grepstad, Physical Review B **84** (22), 220410 (2011).

[2] M. S. Lee, Doctoral thesis, University of California, Davis (2018).

*ambjorn.bang@ntnu.no